Effects of water subdroplet location on the start of puffing/micro-explosion in composite fuel-water droplets

Guillaume Castanet, D.V. Antonov, P.A. Strizhak, S.S. Sazhin

International Journal of Heat and Mass Transfer 186 (2022) 122466

Effects of water subdroplet location on the start of puffing/micro-explosion in composite fuel-water droplets

G. Castanet[a], D.V. Antonov[b], P.A. Strizhak[b], S.S. Sazhin[c,*]

[a] Université de Lorraine, CNRS-UMR7563, CS 25233, France
[b] National Research Tomsk Polytechnic University, 30, Lenin Avenue, Tomsk, 634050, Russia
[c] Advanced Engineering Centre, School of Architecture, Technology and Engineering, University of Brighton, Brighton, BN2 4GJ, UK

Keywords:
Heating
Evaporation
Composite droplets
Puffing
Micro-explosion

A B S T R A C T

A new approach to the verification of the predictions of the earlier developed model of puffing/micro-explosion is suggested, based on the implementation in the numerical code of the analytical solution to the heat transfer equation within a composite droplet. Verification is based upon a comparison between the predictions of the numerical code with this model and those of a fully numerical solution to the equation (the heat transfer module available from COMSOL software). The agreement between the predictions of both codes supports both approaches to the problem. The model is generalised to consider the shifting of the water subdroplet away from the centre of the fuel droplet. This generalisation is based on the numerical solution to the heat transfer equation in the composite droplet taking into account this shift. The start of puffing/micro-explosion in the generalised model is related to the time instant when the temperature at the point of the water/fuel interface closest to the surface of the fuel droplet reaches the water nucleation temperature. The shift is characterised by the distance between the centres of the water subdroplet and the fuel droplet. It is shown that even if this distance is half of the maximal possible distance, the errors in times to puffing/micro-explosion obtained using the original and generalised models do not exceed 5%, which can be tolerated in most practical applications.

1. Introduction

The importance of puffing (swelling and break-up of droplets into several small droplets) and micro-explosion (break-up of droplets producing a cloud of aerosols) in composite fuel-water droplets has been widely discussed [1]. Numerous experimental studies of the phenomena (e.g. [2–4]) were complemented by extensive developments of the models of various levels of complexity.

The most complex models of this phenomenon are based on Direct Numerical Simulation (DNS) [5–7]. Several simplified models (e.g. [8–12]) are focused on the investigation of specific aspects of the phenomena and essentially complement the approaches based on DNS. The model developed by the authors of [12] assumes that a spherical water subdroplet is positioned exactly in the centre of a spherical fuel droplet, as illustrated in Fig. 1.

Puffing/micro-explosion in this model is initiated when the temperature at the fuel-water interface becomes equal to the water nucleation temperature, which takes into account the superheating of water which retards initiation of the phonomena. This model uses the analytical solution to the transient heat transfer equation in a fuel-water droplet, with the Robin boundary condition at the droplet surface. This solution was implemented into a numerical code and used at each time step. The effects of evaporation, using the model developed by Abramzon and Sirignano [13], and swelling were also considered.

This model was extended using a non-self-consistent approach to the case of moving droplets to consider the effects of movement on the values of Sherwood and Nusselt numbers but not on the internal liquid recirculation inside droplets [14]. This extended model proved to be effective in many applications including our recent investigations of puffing/micro-explosion in two and three droplets in a raw, one behind the other [15,16]. At the same time, it has several important weaknesses.

Firstly, the verification of the model was limited by the development of two separate numerical codes, using Wolfram Mathematica v 12.1 and Matlab R2020a, in which the analytical solution to the heat transfer equation in a fuel-water droplet was implemented. Although these codes predicted the same results, both results could be wrong if there is something wrong with the analytical solution.

* Corresponding author.
E-mail address: S.Sazhin@brighton.ac.uk (S.S. Sazhin).

Nomenclature

English symbols

$B_{M(T)}$	Spalding mass (heat) transfer number [-]
c	Specific heat capacity [J/(kg K)]
D	Diffusion coefficient [m^2/s]
g	Acceleration due to gravity [m/s^2]
Gr	Grashov number [-]
h	Convection heat transfer coefficient [$W/(m^2\ K)$]
k	Thermal conductivity [W/(m K)]
L	Distance between the centres of water subdroplet and fuel droplet [m]
$\mathcal{L}$	Specific heat of evaporation [J/kg]
Le	Lewes number [-]
M	Molar mass [kg/kmole]
$\dot{m}_d$	Evaporation rate [kg/s]
Nu	Nusselt number [-]
Pr	Prandtl number [-]
$\dot{q}_d$	Heating rate [W]
r	Radial coordinate [m]
R	Distance from the droplet centre [m]
R_d	Droplet radius [m]
S	$L/L_{\max}$ [-]
Sc	Schmidt number [-]
Sh	Sherwood number [-]
t	Time [s]
T	Temperature [K]
X	Molar fraction [-]
Y	Mass fraction [-]
z	Axial coordinate [m]

Greek symbols

ϑ	Azimuthal coordinate [rad]
κ	Thermal diffusivity [m^2/s]
ν	Kinematic viscosity [m^2/s]
ρ	Density [kg/m^3]
τ_p	Time to puffing/micro-explosion [s]

Subscripts

av	Average
B	Boiling
d	Droplet
eff	Effective
f	Fuel
g	Ambient gas (air)
N	Nucleation
ref	Reference
s	Surface
v	Vapour
w	Water or Water-fuel interface
0	Initial
∞	Ambient conditions

Secondly, the sensitivity of the results to the shifting of the water subdroplet away from the centre of the fuel droplet has not been investigated, and if, for example, the prediction of the model can be applied only to cases when this shift is less than 1%, this model would not be applicable to most practical engineering problems.

Thirdly, no quantitative estimates of the effect of this shift on predicted and observed times to puffing/micro-explosion were made. It was only observed that in most cases these times predicted by the model described in [12], or its extended version, are longer than those observed experimentally. This was related to the shift of the water subdroplet from the centre of the fuel droplet (cf. Fig. 1). However, no quantitative estimates have been made.

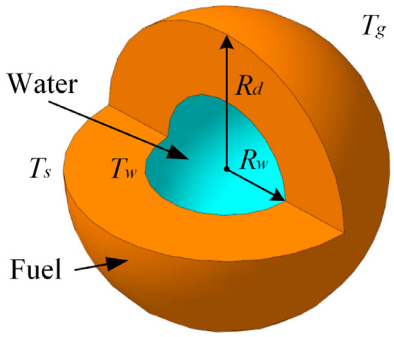

Fig. 1. The position of the water subdroplet in a fuel droplet in the model developed in [12].

The aim of this paper is to address these three issues. As in our previous papers, the problem of the formation of composite droplets will not be considered (e.g. [17,18]).

A new approach to the verification of the predictions of the extended version of the model developed in [12] (hereafter called the Centre Model (CM)) is presented in Section 2. The basis of this verification is a comparison of the predictions of CM with those of a numerical code for solving the same heat transfer problem in the fuel-water droplet. In Section 3, the Centre Model is generalised to consider a shift of the water subdroplet away from the centre of the fuel droplet. This generalisation (hereafter referred to as the Shift Model (SM)) is based on the numerical solution to the heat transfer equation in a fuel-water droplet. In the same section, the errors made using the Centre Model when the water subdroplet is not perfectly centred are investigated. The predictions of the Shift Model are compared with the results of experimental observations in Section 4. The most important findings of the paper are summarised in Section 5.

2. The verification of the centre model

The verification of the Centre Model (CM) was performed by comparing its predictions with those of the modified version of this model (Modified Centre Model, MCM) in which the analytical solution to the heat transfer equation in a fuel-water droplet is replaced with its numerical solution. The latter was obtained using the heat transfer module of COMSOL Multiphysics which contains numerical tools for the simulation of heat conduction and convection based on the finite element methods [15,16,19,20]. The description of the heat transfer inside a composite fuel-water droplet relied on several simplifications. One of these is that the shear force due to the ambient air flow and the internal circulation it can induce in the droplet were not considered. This approximation allowed us to solve a problem of pure heat conduction inside a composite droplet. In the case of a perfectly centred water subdroplet, the modelling approach for both CM and MCM was based on the same set of equations as in [12]. The main equations of this problem are briefly summarised below considering a spherically symmetric problem:

$$\frac{\partial T}{\partial t} = \frac{1}{R^2}\frac{\partial}{\partial R}\left(\kappa R^2 \frac{\partial T}{\partial R}\right), \tag{1}$$

where R is the distance from the centre of the droplet, T temperature, t time,

$$\kappa = \begin{cases} \kappa_w = k_w/(c_w \rho_w) & \text{when} \quad R \le R_w \\ \kappa_f = k_f/(c_f \rho_f) & \text{when} \quad R_w < R \le R_d \end{cases} \tag{2}$$

$\kappa_{w(f)}$, $k_{w(f)}$, $c_{w(f)}$, and $\rho_{w(f)}$ are the water (fuel) thermal diffusivity, thermal conductivity, specific heat capacity, and density, respectively. Both CM and MCM are based on the resolution of Eq. (1) with the following initial condition:

$$T|_{t=0} = \begin{cases} T_{w0}(R) & \text{when} \quad R \le R_w \\ T_{f0}(R) & \text{when} \quad R_w < R \le R_d \end{cases} \tag{3}$$

and boundary conditions at the fuel-water interface and the droplet surface:

$$T|_{R=R_w^-} = T|_{R=R_w^+}, \quad k_w \left.\frac{\partial T}{\partial R}\right|_{R=R_w^-} = k_f \left.\frac{\partial T}{\partial R}\right|_{R=R_w^+}, \tag{4}$$

$$h\,(T_{\text{eff}} - T(R_d)) = k_f \left.\frac{\partial T}{\partial R}\right|_{R=R_d^-}, \tag{5}$$

where h is the convection heat transfer coefficient and T_{eff} is an "effective" ambient gas temperature which takes into consideration the effects of droplet evaporation:

$$T_{\text{eff}} = T_g + \frac{\mathcal{L}\,\dot{m}_d}{4\pi R_d^2\, h}. \tag{6}$$

Condition (5) is the Robin boundary condition.

The droplet evaporation rate $\dot{m}_d$ is determined by the expression:

$$\dot{m}_d = -4\pi R_d\, \rho_{\text{total}}\, \ln(1 + B_M), \tag{7}$$

where $B_M = (Y_{vs} - Y_{v\infty})/(1 - Y_{vs})$ is the Spalding mass transfer number, Y_{vs} ($Y_{v\infty}$) is the mass fraction of fuel vapour at the droplet surface (ambient conditions), D_v is the vapour/gas diffusion coefficient. The dependence of total density of the mixture of ambient gas (air) and fuel vapour $\rho_{\text{total}} = \rho_g + \rho_v$ on R was not considered. The heat transfer coefficient h is defined as:

$$h = k_g Nu/(2R_d), \tag{8}$$

where Nu is the Nusselt number, estimated as:

$$Nu = 2\frac{\ln(1 + B_T)}{B_T}, \tag{9}$$

$$B_T = \frac{c_{pv}(T_g - T_s)}{\mathcal{L}(T_s) - (\dot{q}_d/\dot{m}_d)} \tag{10}$$

is the Spalding heat transfer number, T_g (T_s) gas (surface) temperature, $\mathcal{L}$ specific heat of evaporation, c_{pv} specific vapour heat capacity at constant pressure, $\dot{q}_d$ heat penetrating into the droplet. When deriving (9), droplets were assumed stationary, which implies that the Spalding numbers B_T and B_M are related as:

$$B_T = (1 + B_M)^{\varphi} - 1, \tag{11}$$

where

$$\varphi = \left(\frac{c_{pv}}{c_{pg}}\right)\frac{1}{Le}, \tag{12}$$

$Le = k_g/\left(c_{pg}\,\rho_{\text{total}}\,D_v\right)$ is the Lewis number.

In the CM [12], the analytical solution to the above problem was expressed as an infinite series. This was evaluated at each time step using numerical code to obtain the temperature field distribution inside the droplet. In the MCM, the finite element method was applied using COMSOL Multiphysics to resolve the same problem numerically. An unstructured mesh of about 500 triangular elements was generated for the discretisation of the space.

Both CM and MCM were used to analyse heating and evaporation of a composite n-dodecane/water droplet leading to its puffing/micro-explosion. The following input parameters were used:

- The droplet initial radius and temperature were assumed equal to 5 μm and 300 K, respectively.
- The volume fraction of water was taken equal to 15%.
- Ambient gas temperature and pressure were taken equal to 700 K and 101325 Pa, respectively.
- The approximations of the thermodynamic and transport properties of n-dodecane and distilled water (based on [24]) used in the calculations are given in Appendix B.

In the CM approach, the temperature dependence of the physical properties (namely ρ, c_p and k) was taken into account by updating their values at each time step in the analytical solution. For the MCM approach, the values of the physical properties were evaluated from the temperature field calculated at the previous time step. The variation of the properties in space was directly dealt with by the COMSOL numerical solver.

In both CM and MCM, the water nucleation temperature T_N at the n-dodecane-water interface, at which puffing/micro-explosion is expected to start, was estimated as [12]:

$$T_N = T_B + 12 \times \tanh(\dot{T}/50); \qquad 0 \le \dot{T} \le 300 \ \text{K/s}, \tag{13}$$

$$T_N = 385 + 160 \times \tanh(\dot{T}/10^5) \qquad 10^2 \le \dot{T} \le 10^6 \ \text{K/s}, \tag{14}$$

$$T_N = T_B + 0.37\, T_B \cdot \dot{T}^{\,10/Ja_{HN}} \qquad 10^5 \le \dot{T} \le 10^9 \ \text{K/s}, \tag{15}$$

where $Ja_{HN} = 626$ for water, T_B is the boiling temperature of water in K, $\dot{T}$ is the rate of change of the temperature at the fuel-water interface in K/s.

Plots of droplet average (T_{av}) and surface (T_s) temperatures and the temperature at the fuel-water interface (T_w) versus time, predicted by both codes are shown in Fig. 2a. The corresponding plots showing $\dot{T}_w$ at this interface are presented in Fig. 2b.

As follows from Fig. 2, the results obtained using the CM and MCM coincide within the accuracy of plotting. Using the results presented in Fig. 2 and Formula (14), the times to puffing (times when $T_w = T_N$) were estimated as 0.465 ms (CM) and 0.464 ms (MCM). This shows that the difference between the results is only 0.2% which allows us to conclude that these values coincide. Thus both models, CM and MCM, are verified.

Note that when preparing the plots shown in Fig. 2, the reference molar fraction of n-dodecane vapour $X_{v,\text{ref}}$ was estimated as

$$X_{v,\text{ref}} = \frac{X_{v,\infty} + 2X_{v,s}}{3}, \tag{16}$$

where $X_{v,\infty}$ and $X_{v,s}$ are vapour molar fractions in ambient conditions and at the droplet surface, respectively.

Alternatively, the reference molar fraction of n-dodecane vapour can be estimated as [13,25]:

$$X_{v,\text{ref}} = \frac{\frac{Y_{v,\text{ref}}}{M_v}}{\frac{Y_{v,\text{ref}}}{M_v} + \frac{1 - Y_{v,\text{ref}}}{M_g}}, \tag{17}$$

where $Y_{v,\text{ref}}$ is the reference mass fraction of n-dodecane vapour inferred from the following relation:

$$Y_{v,\text{ref}} = \frac{Y_{v,\infty} + 2Y_{v,s}}{3}, \tag{18}$$

$M_v(M_g)$ is the vapour (air) molar mass. $Y_{v,\infty}$ and $Y_{v,s}$ are vapour mass fractions in ambient conditions and at the droplet surface, respectively.

The same plots as in Fig. 2, but using the previous two expressions for $X_{v,\text{ref}}$ (16) and (17), are presented in Fig. 3. As can be seen in Fig. 3, although the results obtained using Expressions (16) and (17) are slightly different, the closeness between the curves allows us to use either expression for practical applications.

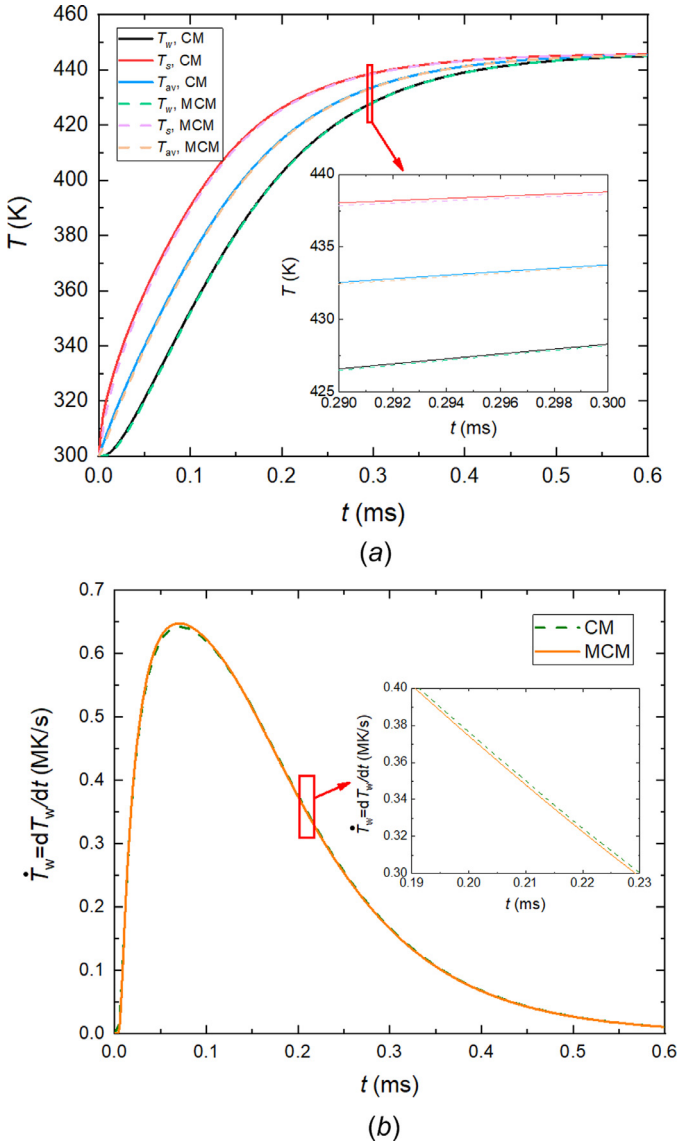

Fig. 2. (a) Plots of droplet average (T_{av}) and surface (T_s) temperatures and the temperature at the n-dodecane-water interface (T_w) versus time, (b) plots of $\dot{T}_w$ at the n-dodecane-water interface versus time. The curves CM and MCM refer to the results predicted by the Centre Model and Modified Centre Model, respectively.

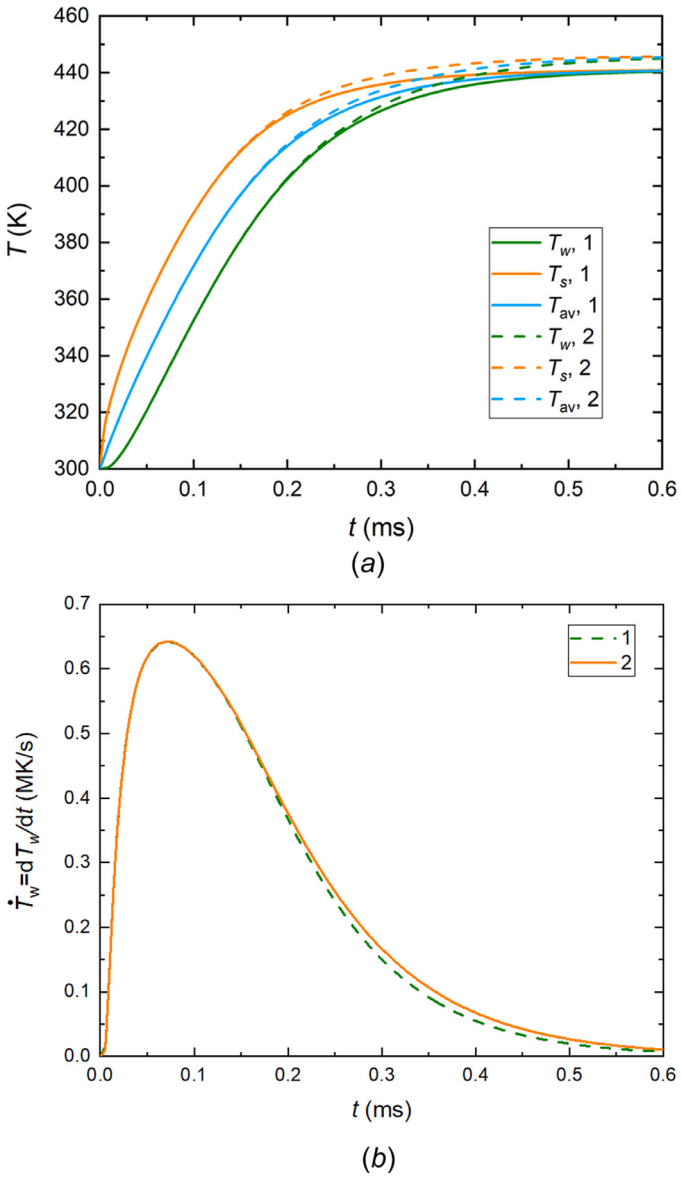

Fig. 3. (a) Plots of droplet average (T_{av}) and surface (T_s) temperatures and the temperature at the n-dodecane-water interface (T_w) versus time, (b) plots of $\dot{T}_w$ at the n-dodecane-water interface versus time. Curves 1 and 2 refer to the results obtained using Expressions (16) and (17), respectively. The calculations were performed using CM.

In the results shown in Figs. 2 and 3, the variation of the droplet radius due to fuel vaporisation and thermal expansion was ignored. R_d and R_w were kept constant, while the vapour mass flow rate $\dot{m}_d$ was evaluated based on Expression (7). In fact, the size variation due to thermal swelling and vaporisation has very limited influence on the time required to reach the nucleation temperature at the n-dodecane-water interface for the conditions used in Figs. 2 and 3. The same observation was made in [12] for rather similar conditions. If required, the radii of the fuel droplets and water subdroplets (R_d and R_w) could be evaluated at each time step using the requirement of conservation of masses of n-dodecane and water (see Eq. (13) in [12]).

3. Description of the shift model

The Modified Centre Model (MCM) presented in Section 2 was generalised to consider possible shifts of the location of the water subdroplet from the centre of the fuel droplet. The geometry used in this generalised Modified Centre Model, called the Shift Model (SM), is shown in Fig. 4. The heat transfer equation (Eq. (1)) was generalised and rewritten in the cylindrical coordinate system (r, ϑ, z), with the z-axis being the line joining the centre of the fuel droplet to that of the water subdroplet, as shown in Fig. 4. The axisymmetric approximation was used with the symmetry condition at $r = 0$:

$$\frac{\partial T}{\partial r} = 0. \tag{19}$$

The main simplifying assumption used in the SM is that the surface temperature of the fuel droplet is uniform although it can change with time. In this case, Eqs. (6)–(12) can be used without further restriction. The boundary conditions at the droplet surface ($R = R_d$) are written as:

$$\int_{-R_d}^{R_d} \left.\frac{\partial T}{\partial R}\right|_{R=R_d^-} dz = \frac{\dot{q}_d}{2\pi R_d k_f} \tag{20}$$

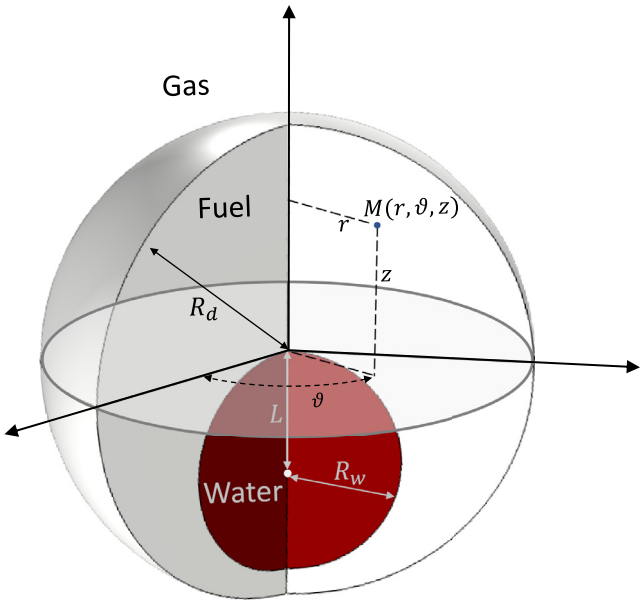

Fig. 4. Schematic presentation of the geometry used in the Shift Model.

$$\left.\frac{\partial T}{\partial z}\right|_{R=R_d} = 0. \tag{21}$$

Equation (21) indicates that temperature T_s at the droplet surface is uniform. The change in this temperature with time was controlled by the average heat flux $\dot{q}_d$ determined by Eq. (20). Note that the spatial distribution of the heat flux at the droplet surface, required to maintain a uniform temperature at the fuel droplet surface, is not specified in Eq. (20). While T_s is uniform, the spatial distribution of the heat flux is not necessarily uniform. Due to the shift in location of the water subdroplet, there is no longer a spherical symmetry to the problem. The value of $\dot{q}_d$ in Eq. (20) can be obtained from the vapour mass flow rate $\dot{m}_d$, or using the effective ambient temperature T_{eff}:

$$\begin{aligned}\dot{q}_d &= |\dot{m}_d|\ \tfrac{c_{pv}(T_g-T_s)}{B_T} - \mathcal{L}(T_s)\\ &= 4\pi R_d^2 \cdot h \cdot\ (T_{\text{eff}} - T_s).\end{aligned} \tag{22}$$

The Shift Model presented above reduces to the MCM as a limiting case when the water subdroplet is perfectly centred ($L = 0$). In that case, (20) reduces to Eq. (5). For the numerical resolution, difficulties are encountered in satisfying the integral boundary condition (20) within the constraints of a uniform surface temperature (Eq. 21). These difficulties, however, were overcome by using the linearity of the heat conduction problem. The approach which we used is similar to that described by Abramzon and Sirignano [13] for solving the energy equation in the Hill vortex model (see Eqs. (40)–(44) in [13]). In their paper, due to the advection of a Hill vortex, a temperature field with no spherical symmetry is assumed, while a uniform temperature is imposed at the droplet surface. The heat conduction problem is decomposed into two problems, making it more straightforward to solve, with a uniform temperature imposed at the droplet surface (Dirichlet condition). See Appendix A for more details.

The shift in the position of the water subdroplet considered in the SM is described by parameter L, the distance between the centre of the water subdroplet and the fuel droplet, shown in Fig. 4. The maximal value of L is $L_{\max} = R_{d0} - (R_{w0}/2)$, where R_{d0} and R_{w0} are the initial values of fuel droplet and water subdroplet radii, respectively. For our analysis, we introduced the normalised shift (S)

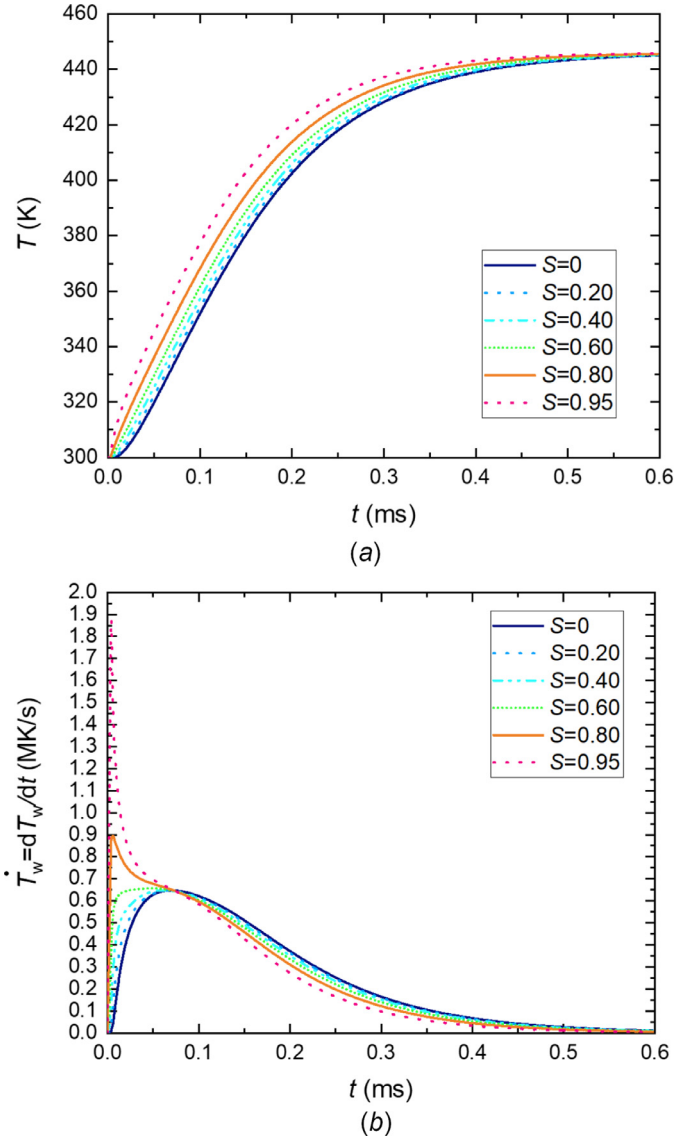

Fig. 5. (a) Plots of the maximal temperature at the n-dodecane-water interface (T_w) versus time for several values of S, (b) plots of $\dot{T}_w$ at the n-dodecane-water interface, at the shortest distance from the fuel droplet surface, versus time for several values of S. Calculations were based on Expression (18). The same values of input parameters as in Figs. 2 and 3 were used.

defined as:

$$S = \frac{L}{L_{\max}}. \tag{23}$$

The main consequence of this shift is that the heating of the fuel-water interface in this case depends on the distance between the droplet surface and this interface. The maximal heating rate is expected at the point closest to the droplet surface. One would expect that the temperature at this point on the interface will be the first to reach the water nucleation temperature, leading to the initiation of puffing/micro-explosion at this location.

Plots of the maximal temperature at the fuel-water interface T_w versus time for several S are presented in Fig. 5a. As follows from this figure, for any given time instant T_w increases with increasing S as expected.

Plots of $\dot{T}_w$ versus time at the fuel-water interface, at the shortest distance from the fuel droplet surface are presented in Fig. 5b for several values of S. As can be seen in this figure, the dependence of $\dot{T}_w$ on S is more complex than that of T_w. At times shorter

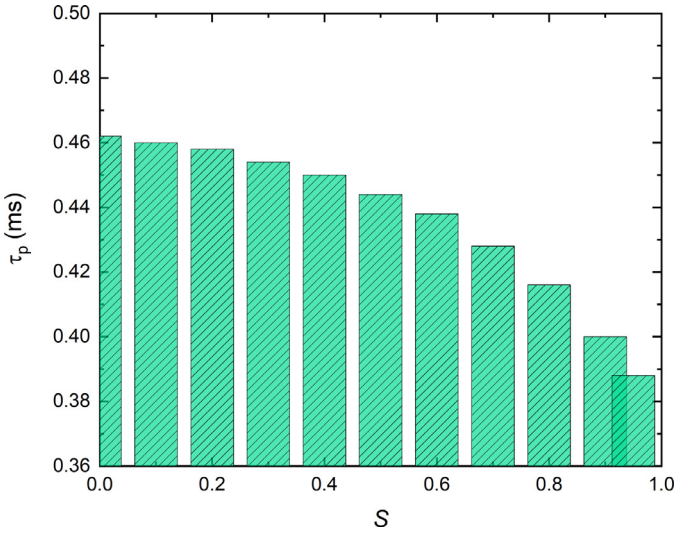

Fig. 6. Times to puffing/micro-explosion at various S inferred from the results presented in Fig. 5 and Formulae (14) and (13).

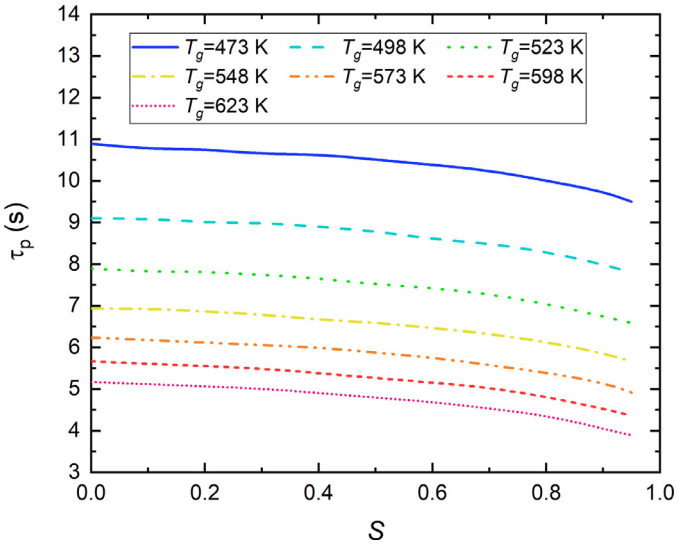

Fig. 7. Times to puffing/micro-explosion versus S at various gas temperatures T_g for droplets with initial radii $R_{d0} = 0.85$ mm.

than about 0.1 ms, $\dot{T}_w$ increases with increasing S, while at times longer than about 0.1 ms, $\dot{T}_w$ decreases with increasing S. At the short times, the heat diffusion inside the droplet is very limited, which leads to large temperature gradients and temporal variations in the temperature at the droplet surface and in its proximity.

Using the results presented in Fig. 5 and Correlations (13)–(15) the time instants when $T_w = T_N$ were obtained for various S. These time instants are known as times to puffing/micro-explosion τ_p. The values of τ_p for various S are presented in Fig. 6. As follows from this figure, the values of τ_p decrease by less than 1% when S increases from 0 to 0.2. This means that the model developed by the authors of [12] (CM) can be safely used when S is less than 0.2. If errors up to 5% can be tolerated, then this model can be used for cases when the shifts are as high as 0.5. For all cases shown in Fig. 6, it should be noted that $\tau_p > 0.38$ ms. As can be seen in Fig. 5b, at these times $\dot{T}_w < 10^5$ K/s. Hence, Correlation (14), or even (13), can be used for the estimation of T_N.

As a second example, plots of times to puffing/micro-explosion versus S are shown in Fig. 7 for droplets with initial radii $R_{d0} =$ 0.85 mm and various ambient gas temperatures T_g. The initial droplet temperature was assumed equal to 300 K. The volume fraction of water was assumed equal to 10% and the ambient gas pressure was fixed at 101325 Pa. As in the case of the previous figures, the transport and thermodynamic properties of n-dodecane and distilled water presented in [24] were used. When estimating the values of τ_p shown in Figure 7, the values of $\dot{T}_w$ were less than 300 K/s. Thus, Correlation (13) was used for estimating T_N. As follows from Figure 7, for all temperatures τ_p slowly decreases with increasing S. When S increases from 0 to $S = 0.3$, a maximal decrease of 3% in τ_p was observed for $T_g = 623$ K. This result is consistent with the one shown in Fig. 6. As follows from Figs. 6 and 7, the errors in estimating τ_p using the Centre Model do not exceed 5% even in the case of a large shift $S = 0.5$. In many applications, this can be tolerated in practical estimations of this parameter.

4. The predictions of the shift model versus experimental data

In this section, the predictions of the Shift and Centre models are compared with experimental data obtained at Tomsk National Research Polytechnical University. The experiments took place in a heated furnace where the droplets were supported by a nickel-chromium alloy wire of 0.2 mm diameter as in the experimental setup described in [21]. The initial droplet temperature was 300 K; the initial droplet radii were in the range 0.65 mm to 0.95 mm. The ambient pressure was atmospheric, taken equal to 101325 Pa; the gas temperatures were in the range 430 K to 850 K. The normalised shift S was inferred from direct observations with errors 5–10% when S varied from 0 to 0.75. Note that our estimations of the shift S were made at $t = 0$ s. However, during droplet heating, the water subdroplet could move from its start point due to the effect of natural convection, which induced circulation flows in the gas and liquid phases.

Note that in some of our experiments several water subdroplets were observed inside single fuel droplets [22]. The analysis of these cases, however, is beyond the scope of this paper.

Two examples of observations of the evolution of the shapes of composite Diesel fuel-water droplets before and during puffing/micro-explosion, using this setup, are demonstrated in Fig. 8. In both cases, the time to puffing was considered to be the time instant when the first child droplet is separated from the parent droplet. This time instant was sometimes well separated from that when micro-explosion was observed as illustrated in Fig. 8a. In these cases some caution would be required when the Centre Model is applied to the interpretation of experimental data as this model assumes that micro-explosion follows puffing without delay. In this case time to puffing/micro-explosion can be referred to as time to puffing.

When applying the Shift Model to the analysis of these data, we need to keep in mind that the difference between the droplet surface temperature and ambient temperature in the presence of gravity leads to the development of natural convection. This convection was considered in the expressions for the Nusselt (Nu) and Sherwood (Sh) numbers using the following formulae [23]:

$$Nu = 2 + \frac{(Nu_0 - 2)}{F_T} \cdot \frac{\ln(1 + B_T)}{B_T}, \tag{24}$$

$$Sh = \left[2 + \frac{(Sh_0 - 2)}{F_M} \cdot \frac{\ln(1 + B_M)}{B_M}\right], \tag{25}$$

$$Nu_0 = 2 + 0.6Gr^{0.25}Pr^{0.33}, \tag{26}$$

$$Sh_0 = 2 + 0.6Gr^{0.25}Sc^{0.33}, \tag{27}$$

$$F_{M(T)} = \left(1 + B_{M(T)}\right)^{0.7} \cdot \frac{\ln\left(1 + B_{M(T)}\right)}{B_{M(T)}}. \tag{28}$$

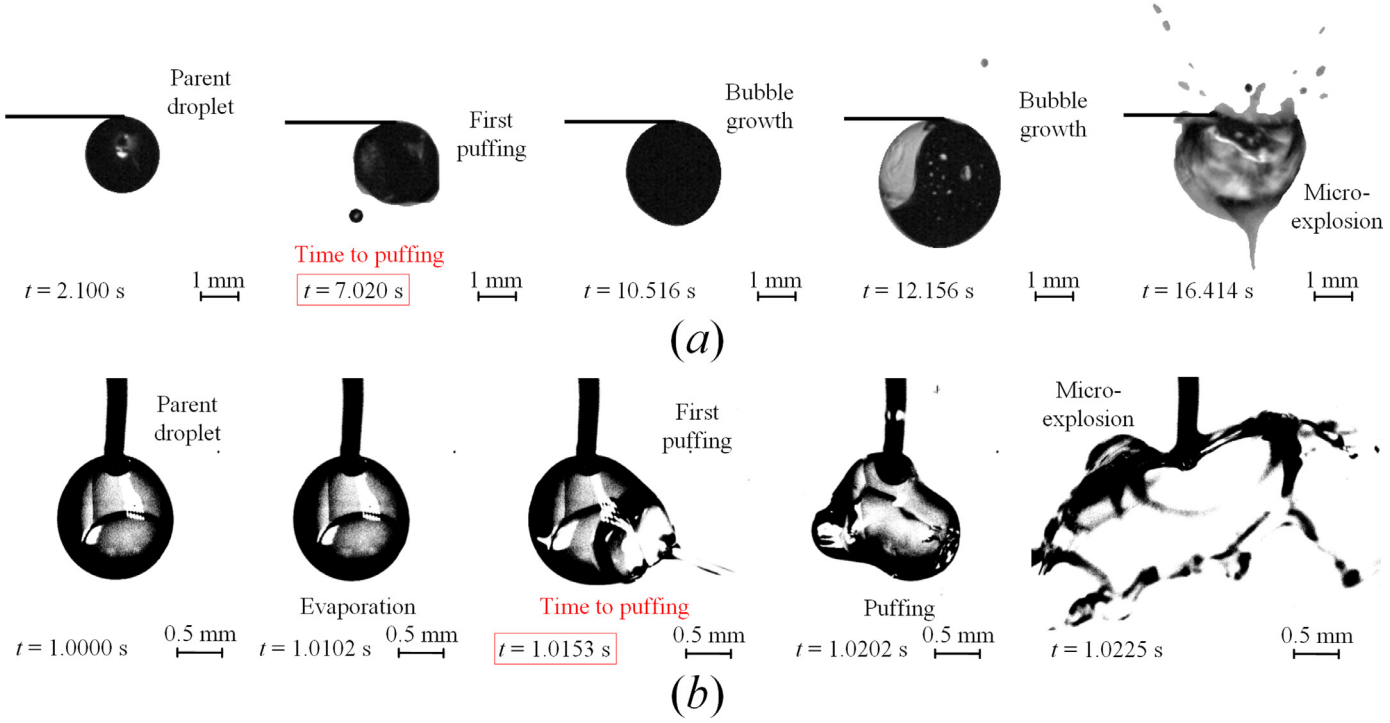

Fig. 8. Typical video frames showing the evolution of shapes of Diesel fuel-water droplets before and during puffing/micro-explosion. (a) Droplet with initial radius $R_{d0} = 0.90$ mm and $S = 0.75$, introduced into a gas at temperature $T_g = 473$ K. (b) Droplet with $R_{d0} = 0.65$ mm and $S = 0.52$, introduced into a gas at temperature $T_g = 850$ K. In all cases, the water volume fractions were 10%, the initial droplet temperatures were 300 K, and ambient gas pressure was atmospheric (assumed equal to 101325 Pa).

where Gr is the Grashof number:

$$Gr = \frac{g(2R_d)^3|T_g - T_s|}{\nu^2\, T_s},$$

Pr and Sc are Prandtl and Schmidt numbers, respectively, ν is the kinematic ambient gas viscosity, g is the acceleration due to gravity, B_M (B_T) are Spalding mass (heat) transfer numbers.

Expressions (26) and (27) were used in both the Centre Model (CM) and the Shift Model (SM). Diesel fuel was approximated by n-dodecane. Only changes in T_s were considered in both CM and SM, while the changes in R_d due to evaporation and thermal swelling were ignored. As follows from further analyses with CM, the effects of the change in R_d on time to puffing/micro-explosion are small and can be ignored in most applications [26,27]. Hence, the assumption of constant R_d is not expected to affect the comparison of CM and SM predictions with experimental results.

Special care was taken to evaluate the shifting of the water subdroplet in the experiments. Planar laser-induced fluorescence (PLIF) was applied to find the position of the water subdroplet with a high degree of accuracy. As in the experiments discussed by Antonov et al. [28], rhodamine B was added to water (1000 μg/l) prior to the preparation of the composite droplet. Since rhodamine B is not miscible in the fuel, only the water subdroplet emits a fluorescent signal when illuminated by the laser. In addition, a shadowgraphy technique using a high-speed camera provided sharp images of the droplet edge. The centroids of the water subdroplet and the fuel droplet were determined using a homemade image analysis program based on Matlab software and its image processing toolbox. Then, the shift L between the two centroids (fuel droplet and water subdroplet) was calculated as illustrated in Fig. 9.

PLIF visualisation of the water subdroplet was performed before heating started. This allowed us to estimate the values of L used in the Shift Model. This shift was assumed to remain unchanged until at least the time when puffing/micro-explosion occurred. In several experiments, however, some movements of the water subdroplet could be observed, which may lead to differences between the model predictions and the results of the experiments.

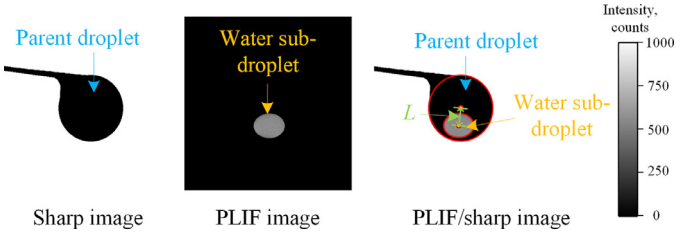

Fig. 9. A typical image of a fuel-water droplet obtained by shadowgraphy with a high-speed camera (left); image of a water subdroplet obtained using the PLIF technique with water seeded with rhodamine B (middle). Once the centres of the fuel droplet and the water subdroplet were identified, the distance L was estimated as shown in (right).

The observed times to puffing/micro-explosion and those predicted by the Centre Model (CM) and Shift Model (SM) for nine cases are presented in Table 1. As follows from this table, in most cases (Cases 1, 2, 3, 5, 6, 7) the values of τ_p predicted by SM are much closer to the experimental data than those predicted by CM. The deviations between the predictions of SM and the experimental results could be partly attributed to considerable uncertainty in the estimation of S using our experimental data, most probably due to movement of the water subdroplet during the experiment. There may also be several other reasons for this, including our assumption that both water subdroplet and fuel droplet are perfectly spherical. In contrast to Cases 1, 2, 3, 5, 6, and 7, for Case 4 the match between the SM predictions and the experimental results is worse than that for CM.

Using S as a tuning parameter, exact matching between the predictions of SM and experimental data was achieved: (S= 0.96 for

Table 1
Times to puffing/micro-explosion (τ_p) observed experimentally (Exp) and predicted by the Centre Model (CM) and Shift Model (SM) for nine cases with the values of R_{d0}, T_g and S shown in the table. In all cases, the initial droplet temperature was 300 K, volume fraction of water was 10%, and ambient gas pressure was atmospheric.

Case	R_{d0} (mm)	T_g (K)	S	τ_p (s) (Exp)	τ_p (s) (CM)	τ_p (s) (SM)
1	0.90	473	0.75	7.02	8.5	7.74
2	0.65	850	0.52	1.02	1.50	1.24
3	0.86	523	0.71	5.11	5.70	5.13
4	0.82	523	0.72	5.11	5.30	4.72
5	0.88	523	0.71	5.14	5.90	5.29
6	0.86	523	0.71	4.90	5.80	5.10
7	0.83	523	0.72	3.74	4.30	3.74
8	0.95	430	< 0.01	14.40	14.50	14.50
9	0.83	623	< 0.01	3.52	3.60	3.60

Case 1, S= 0.75 for Case 2, S= 0.71 for Case 3, S= 0.35 for Case 4, S= 0.77 for Case 5, S= 0.78 for Case 6). For Cases 8 and 9, the water subdroplet was almost exactly in the centre of the fuel droplet. In these cases the predictions of CM and SM coincide and both are reasonably close to experimental data.

5. Conclusions

An approach to the verification of the predictions of the previously developed model of puffing/micro-explosion (see [12]) is suggested. That model uses the assumption that a spherical water subdroplet is located exactly in the centre of a spherical fuel droplet. The analytical solution to the transient heat transfer equation in this droplet, with the Robin boundary condition at its surface, is implemented into a numerical code and used at each time step of the calculations. The time instant when the temperature at the fuel-water interface is equal to the water nucleation temperature is considered to be the start of puffing/micro-explosion. Verification was performed by comparing the predictions of this model with the predictions of the same model, but in which the solution to the heat conduction equation inside the composite droplet was found using the heat transfer module available from COMSOL software (a purely numerical solution to the equation). Agreement between the predictions of both codes supports the validity of both approaches to the problem.

The model suggested in [12] was generalised to consider the shifting of the water subdroplet from the centre of the fuel droplet. This generalisation was based on the numerical solution to the heat transfer equation inside the composite droplet taking into account this shift with other assumptions being the same as in the model in [12]. The start of puffing/micro-explosion in this generalised model is identified with the time instant when the temperature at the point of the fuel-water interface closest to the surface of the fuel droplet becomes equal to the water nucleation temperature. The effects of natural convection on droplet heating and evaporation were considered in both the original and the generalised models.

The size of the shift used in the generalised model is inferred from experimental observations. It is demonstrated that in most cases the time to puffing/micro-explosion predicted by the generalised model is closer to experimental results than that predicted by the original model. The shift is quantified by the normalised shift defined as $S = L/L_{\max}$, where L is the distance from the centre of the water subdroplet to that of the fuel droplet, and $L_{\max} = R_{d0} - (R_{w0}/2)$ ($R_{d0(w0)}$ is the initial radius of the fuel droplet (water subdroplet)) is the maximal value of L. It was shown that for typical values of input parameters for $S \leq 0.2$ the predictions of the original and generalised models differ by less than 1%. For $S \leq 0.5$ this difference increases to 5% which is still acceptable in many engineering applications.

Declaration of Competing Interest

The work described has not been published previously and it is not under consideration for publication elsewhere. Its publication is approved by all authors and tacitly or explicitly by the responsible authorities where the work was carried out. If accepted, it will not be published elsewhere in the same form, in English or in any other language, including electronically without the written consent of the copyright-holder.

CRediT authorship contribution statement

G. Castanet: Conceptualization, Methodology, Resources, Investigation, Software, Writing – review & editing. **D.V. Antonov:** Conceptualization, Methodology, Resources, Investigation, Software. **P.A. Strizhak:** Supervision, Resources, Investigation. **S.S. Sazhin:** Supervision, Conceptualization, Methodology, Writing – review & editing.

Acknowledgments

The authors are grateful: to the Université de Lorraine and the Institut Carnot Icéel for the CALICO (Combustion d'Aérosols Liquides Complexes) grant which supported G. Castanet (who contributed to the development of the model, the simulations and preparation of the text of the paper); for a scholarship from the President of the Russian Federation (Grant SP-447.2021.1) which supported D. Antonov (who performed the experiments, and applied the model to their analysis); to the National Research Tomsk Polytechnic University (project VIU-ISHFVP-60/2019) which supported P.A. Strizhak (who contributed to the analysis of the results); and to the Russian Science Foundation (Grant 21-19-00876), which supported S.S. Sazhin (who contributed to the development of the model, analysis of the results and preparation of the text of the paper).

Appendix A

Assuming that the temperature distribution inside the droplet is known at a certain time t_0, the temperature at the next time step $(t_0 + dt)$ is presented as a linear combination of two functions T_1 and T_2:

$$T(r, z, t) = T_1(r, z, t) + A \cdot T_2(r, z, t). \quad (29)$$

Functions T_1 and T_2 are both obtained by solving the heat transfer equation. They both satisfy the conditions for axi-symmetry (19). T_1 is the solution to a modified problem where the surface temperature does not vary during the time step between t_0 and $t_0 + dt$:

$$T_1(R = R_d, t) = T(R = R_d, t_0) \quad \text{for} \quad t_0 \leq t \leq t_0 + dt. \quad (30)$$

At time t_0, the initial value of the function T_1 is obtained as:

$$T_1(r,z,t_0) = T(r,z,t_0), \tag{31}$$

where $T(r,z,t_0)$ is the temperature distribution in the fuel-water droplet at the last time step of the resolution. The function T_2 represents the effect of a temperature increment of 1 °C at the droplet surface. This function follows from the boundary (surface) and initial conditions:

$$T_2(R = R_d, t) = 1 \quad \text{for} \quad t_0 \le t \le t_0 + dt \tag{32}$$

$$T_2(r,z,t_0) = 0. \tag{33}$$

Finally, the temperature is evaluated from the values of T_1 and T_2 using Eq. (29). The boundary condition (21), corresponding to a uniform surface temperature, is automatically satisfied. The parameter A in Eq. (29) is determined due to the requirement to satisfy the boundary condition (20),

$$A = \frac{\dot{q}_d}{2\pi R_d k_f I_2} - \frac{I_1}{I_2} \tag{34}$$

$$I_1 = \int_{-R_d}^{R_d} \left.\frac{\partial T_1}{\partial R}\right|_{R=R_d^-} dz \text{ and } I_2 = \int_{-R_d}^{R_d} \left.\frac{\partial T_2}{\partial R}\right|_{R=R_d^-} dz \tag{35}$$

The value of A determined by Eq. (34) changes with time. The two partial differential equations for T_1 and T_2 described above were solved numerically based on the finite element method using COMSOL Multiphysics. As for the numerical simulations implemented for the MCM, an unstructured mesh of about 500 triangular elements was generated for the discretisation of the space. One advantage of the proposed decomposition (29) is that functions T_1 and T_2 can be found independently of one another. If the physical properties of water and fuel (n-dodecane) do not vary with time, then the evaluation of T_2 can be performed just once at the beginning of the calculations. In the present case, to deal with the temperature dependence of the physical properties, parameters k, ρ and c in the heat transfer equation were evaluated using the temperature distribution $T(r,z,t_0)$ calculated at the previous time step. Both T_1 and T_2 were calculated as explained above.

Appendix B

Table B.1.

The properties of components used in calculations. T is in K.

Component	Physical properties
water	$\rho_{l,H_2O} = 325 \cdot 0.27^{-\left[1-\left(\frac{T}{647.096}\right)\right]^{0.23}}$ kg/m^3; $C_{l,H_2O} = \left(-2.2417\cdot10^4 + 876.97\cdot T - 2.5704\cdot T^2 + 2.4838\cdot10^{-3}\cdot T^3\right)/18$ J/(kg·K); $k_{l,H_2O} = -0.35667 + 5.057\cdot10^{-3}\cdot T - 6.1071\cdot10^{-6}\cdot T^2$ W/(m·K).
n-dodecane	$\rho_{l,f} = 744.96 - 230.42\cdot\left(\frac{T-300}{300}\right) + 40.9\cdot\left(\frac{T-300}{300}\right)^2 - 88.7\cdot\left(\frac{T-300}{300}\right)^3$ kg/m^3; $C_{l,f} = 2172.5 + 1260.5\cdot\left(\frac{T-300}{300}\right) - 63.38\cdot\left(\frac{T-300}{300}\right)^2 +$ $+45.17\cdot\left(\frac{T-300}{300}\right)^3$ J/(kg·K); $k_{l,f} = 0.1405 - 0.00022\cdot(T-300)$ W/(m·K). $L_{l,f} = 0.03744\cdot(659-T)^{0.38}$ MJ/kg; $M_f = 0.17$ kg/mol; $P_{sat,f}(T) = 10^5\cdot\exp\left(8.1948 - 7.8099\cdot(300/T) - 9.0098\cdot(300/T)^2\right)$ Pa;
n-dodecane vapour	$D_{v,f} = \frac{0.527\cdot(T/300)^{1.583}}{P_{gas}}$ m^2/s; $C_{v,f} = 297.9 + 1439.4\cdot(T/300) - 135.1\cdot(T/300)^2$ J/(kg·K); $\mu_{v,f} = \left(0.5651 + 0.001041\cdot(T-300)\right)\cdot10^{-5}$ Pa·s; $k_{v,f} = 0.02667\cdot\left(\frac{T}{300}\right) - 0.02087$ W/(m·K).
gas	$M_g = 0.029$ kg/mol; $C_g = -0.00000044\cdot T^3 + 0.00092454\cdot T^2 - 0.40771821\cdot T +$ $+1057.29181929$ J/(kg·K); $\mu_g = \left(-0.00019342657\cdot T^2 + 0.58086013986\cdot T + 27.72412587413\right)\cdot10^{-7}$ Pa·s; $k_g = \begin{pmatrix} -0.00000000125\cdot T^4 + 0.00000244918\cdot T^3 - \\ -0.00153675321\cdot T^2 + 0.43343841945\cdot T - \\ -22.50161033466 \end{pmatrix}\cdot10^{-3}$ W/(m·K).
mixture	$\rho_{ref} = \frac{P_{gas}\cdot\left(M_g\cdot X_{g,ref} + M_f\cdot X_{f,ref}\right)}{R_{gas}\cdot T}$ kg/m^3.

References

[1] D. Ogunkoya, S. Li, O.J. Rojas, T. Fang, Performance, combustion, and emissions in a diesel engine operated with fuel-in-water emulsions based on lignin, Appl. Energy 154 (2015) 851–861, doi:10.1016/j.apenergy.2015.05.036.

[2] C. Cen, H. Wu, C. Lee, L. Fan, F. Liu, Experimental investigation on the sputtering and micro-explosion of emulsion fuel droplets during impact on a heated surface, Int. J. Heat Mass Transf. 132 (2019) 130–137, doi:10.1016/J.IJHEATMASSTRANSFER.2018.12.007.

[3] M.M. Avulapati, L.C. Ganippa, J. Xia, A. Megaritis, Puffing and micro-explosion of diesel-biodiesel-ethanol blends, Fuel 166 (2016) 59–66, doi:10.1016/j.fuel.2015.10.107.

[4] O. Moussa, D. Tarlet, P. Massoli, J. Bellettre, Parametric study of the micro-explosion occurrence of w/o emulsions, Int. J. Therm. Sci. 133 (2018) 90–97, doi:10.1016/j.ijthermalsci.2018.07.016.

[5] J. Shinjo, J. Xia, A. Megaritis, L.C. Ganippa, R.F. Cracknell, Modeling temperature distribution inside an emulsion fuel droplet under convective heating: a key to predicting microexplosion and puffing, At. Sprays 26 (2016) 551–583, doi:10.1615/AtomizSpr.2015013302.

[6] J. Shinjo, J. Xia, L.C. Ganippa, A. Megaritis, Physics of puffing and microexplosion of emulsion fuel droplets, Phys. Fluids 26 (2014) 103302, doi:10.1063/1.4897918.

[7] S. Fostiropoulos, G. Strotos, N. Nikolopoulos, M. Gavaises, Numerical investigation of heavy fuel oil droplet breakup enhancement with water emulsions, Fuel 278 (2020) 118381, doi:10.1016/j.fuel.2020.118381.

[8] O.G. Girin, Dynamics of the emulsified fuel droplet micro-explosion, At. Sprays 27 (2017) 407–422, doi:10.1615/AtomizSpr.2017017143.

[9] S.S. Sazhin, O. Rybdylova, C. Crua, M. Heikal, M.A. Ismael, Z. Nissar, A.R.B.A. Aziz, A simple model for puffing/micro-explosions in water-fuel emulsion droplets, Int. J. Heat Mass Transf. 131 (2019) 815–821, doi:10.1016/j.ijheatmasstransfer.2018.11.065.

[10] S. Fostiropoulos, G. Strotos, N. Nikolopoulos, M. Gavaises, A simple model for breakup time prediction of water-heavy fuel oil emulsion droplets, Int. J. Heat Mass Transf. 164 (2021) 120581, doi:10.1016/j.ijheatmasstransfer.2020.120581.

[11] D.V. Antonov, R.M. Fedorenko, G.V. Kuznetsov, P.A. Strizhak, Modeling the micro-explosion of miscible and immiscible liquid droplets, Acta Astronaut 171 (2020) 69–82, doi:10.1016/j.actaastro.2020.02.040.

[12] S.S. Sazhin, T. Bar-Kohany, Z. Nissar, D. Antonov, P.A. Strizhak, O.D. Rybdylova, A new approach to modelling micro-explosions in composite droplets, Int. J. Heat Mass Transf. 161 (2020) 120238, doi:10.1016/j.ijheatmasstransfer.2020.120238.

[13] B. Abramzon, W.A. Sirignano, Droplet vaporization model for spray combustion calculations, Int. J. Heat Mass Transf. 32 (1989) 1605–1618, doi:10.1016/0017-9310(89)90043-4.

[14] D.V. Antonov, P.A. Strizhak, R.M. Fedorenko, Z. Nissar, S.S. Sazhin, Puffing and micro-explosions in rapeseed oil/water droplets: the effects of coal microparticles in water, Fuel 289 (2021) 119814, doi:10.1016/j.fuel.2020.119814.

[15] D.V. Antonov, R.M. Fedorenko, P.A. Strizhak, G. Castanet, S.S. Sazhin, Puffing/micro-explosion of two closely spaced composite droplets in tandem: experimental results and modelling, Int. J. Heat Mass Transf. 176 (2021) 121449, doi:10.1016/j.ijheatmasstransfer.2021.121449.

[16] D.V. Antonov, R.S. Volkov, R.M. Fedorenko, P.A. Strizhak, G. Castanet, S.S. Sazhin, Temperature measurements in a string of three closely spaced droplets before the start of puffing/micro-explosion: experimental results and modelling, Int. J. Heat Mass Transf. 181 (2021) 121837, doi:10.1016/j.ijheatmasstransfer.2021.121837.

[17] P.K. Roy, B.P. Binks, E. Bormashenko, I. Legchenkova, S. Fujii, S. Shoval, Manufacture and properties of composite liquid marbles, J. Colloid Interface Sci. 575 (2020) 35–41, doi:10.1016/j.jcis.2020.04.066.

[18] P.K. Roy, I. Legchenkova, S. Shoval, L.A. Dombrovsky, E. Bormashenko, Osmotic evolution of composite liquid marbles, J. Colloid Interface Sci. 592 (2021) 167–173, doi:10.1016/j.jcis.2021.02.055.

[19] G. Castanet, L. Perrin, O. Caballina, F. Lemoine, Evaporation of closely-spaced interacting droplets arranged in a single row, Int. J. Heat Mass Transf. 93 (2016) 788–802, doi:10.1016/j.ijheatmasstransfer.2015.09.064.

[20] G. Castanet, C. Maqua, M. Orain, F. Grisch, F. Lemoine, Investigation of heat and mass transfer between the two phases of an evaporating droplet stream using laser-induced fluorescence techniques: comparison with modeling, Int. J. Heat Mass Transf. 50 (2007) 3670–3683, doi:10.1016/j.ijheatmasstransfer.2006.08.038.

[21] D.V. Antonov, G.S. Nyashina, P.A. Strizhak, D.S. Romanov, Micro-explosive droplet fragmentation of environmentally promising coal-water slurries containing petrochemicals, Fuel 283 (2021) 118949, doi:10.1016/j.fuel.2020.118949.

[22] D.V. Antonov, M.V. Piskunov, P.A. Strizhak, Breakup and explosion of droplets of two immiscible fluids and emulsions, Int. J. Therm. Sci 142 (2019) 30–41, doi:10.1016/j.ijthermalsci.2019.04.011.

[23] A.P. Pinheiro, J.M. Vedovoto, Evaluation of droplet evaporation models and the incorporation of natural convection effects, Flow Turbul. Combust. 102 (2019) 537–558, doi:10.1007/s10494-018-9973-8.

[24] L.C. Yaws, Yaws handbook of thermodynamic and physical properties of chemical compounds, Knovel, 2003. Electronic ISBN 978-1-59124-444-8

[25] M. Yuen, L. Chen, On drag of evaporating liquid droplets, Combust. Sci. Technol. 14 (1976) 147–154, doi:10.1080/00102207608547524.

[26] J. Wang, X. Qiao, D. Ju, L. Wang, C. Sun, Experimental study on the evaporation and micro-explosion characteristics of nanofuel droplet at dilute concentrations, Energy 183 (2019), doi:10.1016/j.energy.2019.06.136.

[27] S. Shen, K. Sun, Z. Che, T. Wang, M. Jia, Puffing and micro-explosion of heated droplets for homogeneous ethanol-propanol-hexadecane fuel and micro-emulsified ethanol-biodiesel-hexadecane fuel, Appl. Therm. Eng. 165 (2020) 114537, doi:10.1016/J.APPLTHERMALENG.2019.114537.

[28] D.V. Antonov, G.V. Kuznetsov, P.A. Strizhak, Comparison of the characteristics of micro-explosion and ignition of two-fluid water-based droplets, emulsions and suspensions, moving in the high-temperature oxidizer medium, Acta Astronaut. 160 (2019) 258–269, doi:10.1016/j.actaastro.2019.04.048.